

Impact of event activity variable on the ratio observables in isobar collisions

Jiangyong Jia,^{1,2} Gang Wang,³ and Chunjian Zhang¹

¹*Department of Chemistry, Stony Brook University, Stony Brook, NY 11794, USA*

²*Physics Department, Brookhaven National Laboratory, Upton, NY 11976, USA*

³*Department of Physics and Astronomy, University of California, Los Angeles, California 90095, USA*

The STAR isobar data of $^{96}\text{Ru}+^{96}\text{Ru}$ and $^{96}\text{Zr}+^{96}\text{Zr}$ collisions at $\sqrt{s_{\text{NN}}} = 200$ GeV show that ratios of observables ($R_{\mathcal{O}}$) such as the multiplicity distribution, $p(N_{\text{ch}})$, and the harmonic flow, v_n , deviate from unity, when presented as a function of centrality, c [1]. These deviations have been attributed to the differences in the shape and radial profiles between ^{96}Ru and ^{96}Zr nuclei. In addition, the ratios $R_{\mathcal{O}}(x)$ depend on the choice of the event activity variable x , which could be either N_{ch} or centrality. We estimate the difference ΔR between these two choices, based on the published $p(N_{\text{ch}})$, as well as those from a multiphase transport (AMPT) model with varied nuclear structure parameters: nuclear radius (R_0), surface diffuseness (a_0), quadrupole deformation (β_2), and octupole deformation (β_3). In contrary to $R_{v_n}(c)$, $R_{v_n}(N_{\text{ch}})$ is nearly independent of the analysis approaches, suggesting that nonflow effects are better controlled by N_{ch} than c . The ratios of observables sensitive to the chiral magnetic effect (CME) are also much closer to unity for $x = N_{\text{ch}}$ than $x = c$, indicating that the ratios calculated at the same N_{ch} provide a better baseline for the non-CME background. According to the AMPT results, the dominant parameter for ΔR is a_0 , while R_0 and β_n are only important in central collisions. The published $p(N_{\text{ch}})$ is also used to estimate $\Delta R_{\langle p_{\text{T}} \rangle}$ for mean transverse momentum, which is non-negligible compared with $R_{\langle p_{\text{T}} \rangle} - 1$.

PACS numbers: 25.75.Gz, 25.75.Ld, 25.75.-1

The main goal of the isobar collisions ($^{96}\text{Ru}+^{96}\text{Ru}$ and $^{96}\text{Zr}+^{96}\text{Zr}$ at $\sqrt{s_{\text{NN}}} = 200$ GeV) at the Relativistic Heavy Ion Collider (RHIC) is to search for the elusive chiral magnetic effect (CME) [2, 3]. Since ^{96}Ru contains more protons than ^{96}Zr , $^{96}\text{Ru}+^{96}\text{Ru}$ collisions generate stronger initial magnetic fields than $^{96}\text{Zr}+^{96}\text{Zr}$ collisions, leading to potentially detectable differences in the CME sensitive observables, such as the $\Delta\gamma_{112}$ correlator [4]. However, no evidence of the CME signal has been found in the first isobar analysis from the STAR Collaboration [1]. Instead, the search uncovers significant differences in many observables, supportive of the structure differences between the two nuclei [5]. In particular, the collective-flow results reveal large deformations in the two nuclei [6], as well as a difference in the neutron skin [7]. This opens up a new opportunity to probe the collective nuclear structure using high-energy isobar collisions [8]. Ultimately, the effects of nuclear structures [9] and the nonflow backgrounds [10] have to be accounted for, before any residual differences might be attributable to the genuine CME signal.

The collective shape and radial profile of atomic nuclei are often described by a deformed Woods-Saxon (WS) density, separately for protons and neutrons,

$$\rho(r, \theta, \phi) \propto \frac{1}{1 + e^{[r - R_0(1 + \beta_2 Y_2^0(\theta, \phi) + \beta_3 Y_3^0(\theta, \phi))]/a_0}}. \quad (1)$$

The nuclear structure parameterization includes half-density radius (R_0), surface diffuseness (a_0), and axial symmetric quadrupole deformation (β_2) and octupole deformation (β_3). Model studies of elliptic flow (v_2) and triangular flow (v_3) suggest $\beta_2 \sim 0.15$ for ^{96}Ru and $\beta_3 \sim 0.2$ for ^{96}Zr , respectively [6]. In the mid-central collisions, the comparison of v_2 and the multiplicity distribution

between the two isobaric systems supports the idea that ^{96}Zr has a thicker neutron skin than ^{96}Ru [5, 11]. Predictions for other observables and their sensitivities to deformation and neutron skin have also been made, such as mean transverse momentum $\langle p_{\text{T}} \rangle$ [12], $\langle p_{\text{T}} \rangle$ fluctuations [13], and v_n - p_{T} correlations [14–16].

One thing to note is that the observable ratios between the two isobaric systems are usually presented as a function of an event activity variable, which is also affected by the nuclear structure. The STAR measurements use centrality (c) and charged-particle multiplicity (N_{ch}) in the pseudorapidity range of $|\eta| < 0.5$ as the event activity variables. Centrality is calculated directly from the N_{ch} distribution, $p(N_{\text{ch}})$, as $c(N_{\text{ch}}) = \int_{N_{\text{ch}}}^{\infty} p(n) dn$. The $c(N_{\text{ch}})$ function is monotonic with a range of $0 \leq c \leq 1$ (see Fig. 1 for $c(N_{\text{ch}})_{\text{Ru}}$ and $c(N_{\text{ch}})_{\text{Zr}}$). The STAR data show that $p(N_{\text{ch}})$ is broader in Ru+Ru than in Zr+Zr collisions, and thus events in the two collision systems at matching N_{ch} correspond to different or mismatched c values, and vice versa. Therefore, the ratio of a given observable \mathcal{O} relies on the event activity variable x : $R_{\mathcal{O}}(x) = \mathcal{O}(x)_{\text{Ru}}/\mathcal{O}(x)_{\text{Zr}}$, with $x = c$ or N_{ch} . We quantify the effect of mismatched event activity with the first-order approximation,

$$\Delta R_{\mathcal{O}} = \frac{\mathcal{O}(c_{\text{Ru}})_{\text{Ru}} - \mathcal{O}(c_{\text{Zr}})_{\text{Ru}}}{\mathcal{O}(c_{\text{Zr}})_{\text{Zr}}} \approx \frac{\mathcal{O}'(c)}{\mathcal{O}(c)} \Delta c, \quad (2)$$

$$\Delta R_{\mathcal{O}} = \frac{\mathcal{O}(N_{\text{chRu}})_{\text{Ru}} - \mathcal{O}(N_{\text{chZr}})_{\text{Ru}}}{\mathcal{O}(N_{\text{chZr}})_{\text{Zr}}} \approx \frac{\mathcal{O}'(N_{\text{ch}})}{\mathcal{O}(N_{\text{ch}})} \Delta N_{\text{ch}}. \quad (3)$$

Here $\Delta c = c_{\text{Ru}} - c_{\text{Zr}}$, $\mathcal{O}'(c) = d\mathcal{O}(c)/dc$, and similarly for ΔN_{ch} and $\mathcal{O}'(N_{\text{ch}})$. Both Δc and ΔN_{ch} can be directly read off from Fig. 1. Eq. (2) provides the correction from the ratio at matching c to the ratio at matching N_{ch} , while Eq. (3) provides the correction from the ratio at matching N_{ch} to the ratio at matching c . Therefore

these two corrections have the opposite signs. $\Delta R_{\mathcal{O}}$ is proportional to the derivative $\ln'(\mathcal{O}(c)) = \mathcal{O}'(c)/\mathcal{O}(c)$, and hence its sign depends on whether \mathcal{O} increases or decreases with centrality. In the following figures and related discussions, $\Delta R_{\mathcal{O}}$ always denotes the ratio at matching N_{ch} minus that at matching centrality, unless specified otherwise.

In this paper, we apply Eqs. (2) and (3) directly to the published experimental data [1] to estimate the change in the ratio when switching the x -axis between c and N_{ch} . We then investigate the origin of this change using a multiphase transport (AMPT) model [17]. A previous study [5] explains how $p(N_{\text{ch}})$ is influenced by each of the four WS parameters (R_0 , a_0 , β_2 , and β_3). The values of these parameters for the isobaric nuclei are taken from Ref. [5] and listed in Table I. Each scenario of the AMPT study has a relation between c and N_{ch} , similar to the real data in Fig. 1. These relations in turn can be used as input for Eqs. (2) and (3) to estimate the impact of each parameter on $\Delta R_{\mathcal{O}}$, when switching between the centrality dependence and the N_{ch} dependence.

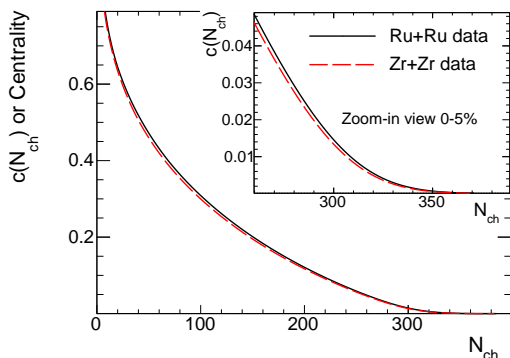


FIG. 1. Centrality vs N_{ch} , i.e. $c(N_{\text{ch}})$ obtained from the published $p(N_{\text{ch}})$ in $^{96}\text{Ru}+^{96}\text{Ru}$ and $^{96}\text{Zr}+^{96}\text{Zr}$ collisions [1]. Similar relations are also obtained in the AMPT model for each variation of WS parameters (not shown).

Species	R_0 (fm)	a_0 (fm)	β_2	β_3
^{96}Ru	5.09	0.46	0.162	0
^{96}Zr	5.02	0.52	0.06	0.20

TABLE I. Collective nuclear structure parameters for ^{96}Ru and ^{96}Zr from Ref. [5].

Figure 2(a) shows $\Delta N_{\text{ch}}(c) = N_{\text{ch,Ru}}(c) - N_{\text{ch,Zr}}(c)$ and Fig. 2(b) shows $\Delta c(N_{\text{ch}}) = c_{\text{Ru}}(N_{\text{ch}}) - c_{\text{Zr}}(N_{\text{ch}})$ as a function of centrality. Note that ΔN_{ch} is calculated at matching c , and Δc is calculated at matching N_{ch} , whose values can be read off directly from Fig. 1 or from analogue plots in the AMPT simulations [5]. Furthermore, the x -axis in all following figures, either centrality or N_{ch} , are always chosen to represent the values obtained for Ru+Ru collisions. Both ΔN_{ch} and Δc can then be presented as a function of either c or N_{ch} . Since the $p(N_{\text{ch}})_{\text{Ru}}$ distribution is broader than $p(N_{\text{ch}})_{\text{Zr}}$, events with the same N_{ch} correspond to larger c values (or more peripheral

collisions) in Ru+Ru than in Zr+Zr. Conversely, events with the same c correspond to larger N_{ch} in Ru+Ru than in Zr+Zr. The overall centrality dependence of ΔN_{ch} and Δc in Fig. 2 can be qualitatively reproduced by the AMPT model after taking into account the influences of all four WS parameters. A previous study [5] has shown that the impact of the four WS parameters on isobar ratios are independent of each other when chosen from Table I. Therefore, the impact of β_2 is reflected by the points represented by label “ β_2 ”, the impact of β_3 is reflected by the change from label “ β_2 ” to label “ $\beta_{2,3}$ ”, the impact of a_0 is reflected by the change from label “ $\beta_{2,3}$ ” to label “ $\beta_{2,3}, a_0$ ”, and so on. We briefly summarize the AMPT results as follows: 1) The diffuseness parameter a_0 has the largest impact on $p(N_{\text{ch}})$, and the smaller a_0 value of Ru tends to make $p(N_{\text{ch}})_{\text{Ru}}$ broader than $p(N_{\text{ch}})_{\text{Zr}}$. 2) Half-density radius R_0 also plays a sizeable role in central collisions, and the larger R_0 of Ru tends to reduce the range of $p(N_{\text{ch}})_{\text{Ru}}$ compared with $p(N_{\text{ch}})_{\text{Zr}}$. 3) The effects of nuclear deformation are mostly concentrated in central collisions, with $\beta_{2\text{Ru}}$ and $\beta_{3\text{Zr}}$ working in the opposite directions.

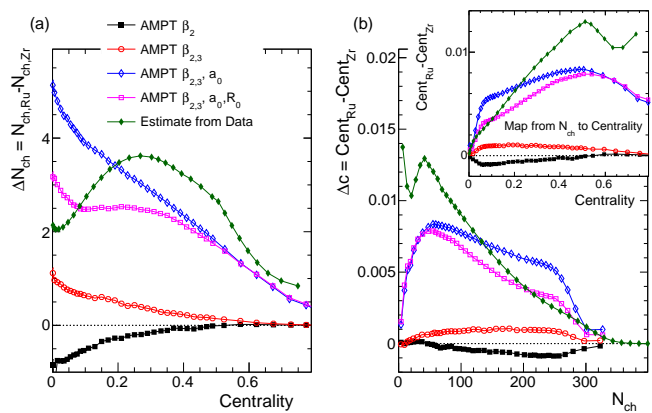


FIG. 2. (a) $\Delta N_{\text{ch}} = N_{\text{ch,Ru}}(c) - N_{\text{ch,Zr}}(c)$ for events at matching centrality for isobar collisions. (b) $\Delta c = c_{\text{Ru}}(N_{\text{ch}}) - c_{\text{Zr}}(N_{\text{ch}})$ for events at matching N_{ch} . Both are obtained directly from Fig. 1. The insert panel shows Δc after mapping N_{ch} to centrality in the x -axis. In comparison with the data, the AMPT calculations are added sequentially to include the effects of β_2 , β_3 , a_0 and R_0 in the two systems in Table I.

Besides Δc , we also need to know the local slope of $\ln(\mathcal{O}(c))$ in Eq. (2), to estimate $\Delta R_{\mathcal{O}}$ when switching from the ratio at matching c to the ratio at matching N_{ch} . Ref. [1] has published results for v_2 , v_3 , and the CME sensitive observables such as $\Delta\gamma_{112}$, $\Delta\delta$, and $\kappa_{112} \equiv \Delta\gamma_{112}/(v_2\Delta\delta)$. We shall not explain the definitions and the physical meanings of these CME related observables (see Ref. [18]), but instead just provide an estimate of $\Delta R_{\mathcal{O}}$ and explore its origin with the AMPT model.

The v_2 and v_3 data in Ref. [1] involve several analysis methods with different sensitivities to nonflow effects. We choose the STAR results from three methods, and display them in the top panels of Fig. 3. The directly-

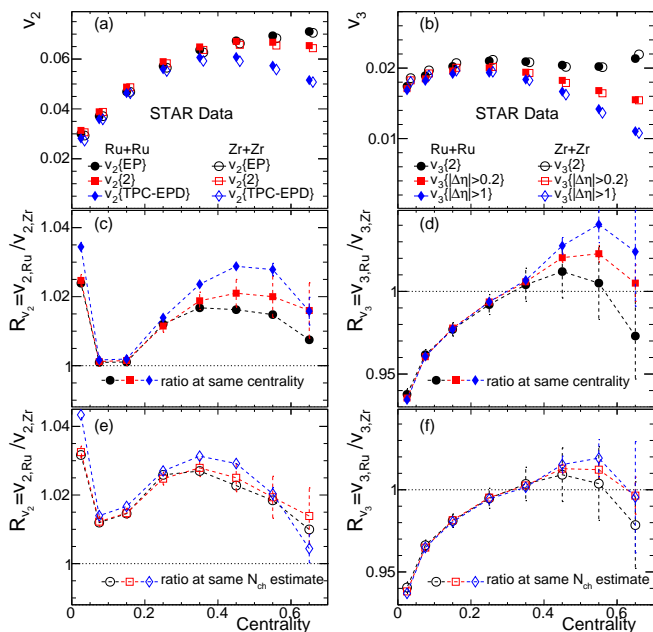


FIG. 3. The STAR v_2 (a) and v_3 (b) data from isobar collisions using three analysis methods from Ref. [1]. The ratios R_{v_2} (c) and R_{v_3} (d) are calculated at matching centrality directly with the v_n data from the top panels. The ratios $R_{v_2}(N_{\text{ch}})$ (e) and $R_{v_3}(N_{\text{ch}})$ (f) are calculated at matching N_{ch} using Eq. (2) with data from Fig. 2 as described in the text.

calculated $R_{v_n}(c)$ ratios are presented as a function of centrality in the middle panels. The bottom panels show the $R_{v_n}(N_{\text{ch}})$ ratios taken at $N_{\text{ch,Ru}}$ for each centrality bin using Eq. (2) with data from Fig. 2. In general, $R_{v_2}(N_{\text{ch}})$ is larger than $R_{v_2}(c)$, since v_2 increases with c , yielding a positive $\ln'(v_2(c))$. In contrast, $R_{v_3}(N_{\text{ch}})$ is nearly the same as $R_{v_3}(c)$, as expected from the weak centrality dependence of v_3 . In peripheral collisions, where v_2 and v_3 are highly affected by nonflow effects, the ratios are method-dependent as expected. Remarkably, the $R_{v_n}(N_{\text{ch}})$ ratios from different methods are much closer to each other than the case of $R_{v_n}(c)$. This suggests that nonflow effects in the two isobaric systems are controlled by N_{ch} instead of centrality. In other words, nonflow contributions in Ru+Ru and Zr+Zr collisions are almost the same at matching N_{ch} , and hence are different at matching centrality.¹

Next, we estimate the impact of the WS parameters on the isobar ratio in the AMPT model using Fig. 2 as input. We select the results whose methods have smaller nonflow, i.e. $v_2\{\text{TPC-EPD}\}$ and $v_3\{|\Delta\eta|>1\}$, and present

¹ In this scenario, the remaining differences in $R_{v_n}(N_{\text{ch}})$ between the analysis methods could be attributed to the dilution effects associated with the different amounts of nonflow effects in those methods. However, the STAR measurements need to be repeated with much finer centrality bins, such that Eq. (2) can provide a more accurate estimate.

them in Fig. 4. The model calculations are compared with the ΔR_{v_n} values estimated from the STAR data, which are just the differences between the open diamonds in the bottom panels and the solid diamonds in the middle panels of Fig. 3. As expected, a_0 plays a leading role in the difference, followed by R_0 , and then β_3 and β_2 . The calculated ΔR_{v_n} after considering all the nuclear structure effects (open boxes) are similar to the data (solid diamonds) for $c < 0.2$, but are smaller in magnitude elsewhere.

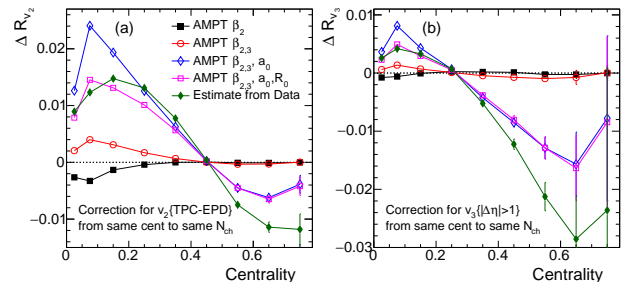


FIG. 4. The difference between the ratio at matching N_{ch} and the ratio at matching centrality: ΔR_{v_2} (a) and ΔR_{v_3} (b), calculated using $p(N_{\text{ch}})$ from the STAR data [1] as well as AMPT including the effects of WS parameters in Eq. (1).

Figure 5 shows the STAR data of the CME sensitive observables: $\Delta\delta$ (a), $\Delta\gamma_{112}$ (b) and $\kappa_{112} \equiv \Delta\gamma_{112}/(v_2\Delta\delta)$ (c). The middle row presents the ratios of Ru+Ru to Zr+Zr for the corresponding observables at matching c and at matching N_{ch} . In the latter case, we have also tried an alternative approach by modifying Eq. (2) to a second-order polynomial interpolation, determined by every three adjacent points (labelled as "estimate2"). The results from the two interpolation methods are nearly identical in central collisions, but show some deviations elsewhere. To improve the accuracy of our estimate, STAR measurements need to be repeated with much finer centrality bins in the future. For most centrality intervals under study, both the $\Delta\delta$ ratios and the $\Delta\gamma_{112}$ ratios change from below unity to above unity after switching from matching c to matching N_{ch} . Such qualitative changes reveal the importance of choosing the proper event activity variable, as this choice may strongly affect the perception of whether/how R deviates from unity, and whether it is attributable to the genuine CME effects. In general, the κ_{112} ratios at matching N_{ch} are consistent with unity, whereas those at matching c are significantly below unity, suggesting that the non-CME backgrounds in the two systems are better controlled by N_{ch} than c . The bottom panels show that the effects of switching the event activity variable tend to be larger in more peripheral collisions, and are dominated by a_0 .

The last set of observables to be studied in this paper are $\langle p_T \rangle$ and its fluctuations in terms of scaled-variance, $\sigma_{p_T}/\langle p_T \rangle$. To estimate $\Delta R_{\mathcal{O}}$ for these observables, we need to express them as a function of N_{ch} (Eq.(3)). Here we assume that the multiplicity dependence of either observable in isobar collisions is similar to

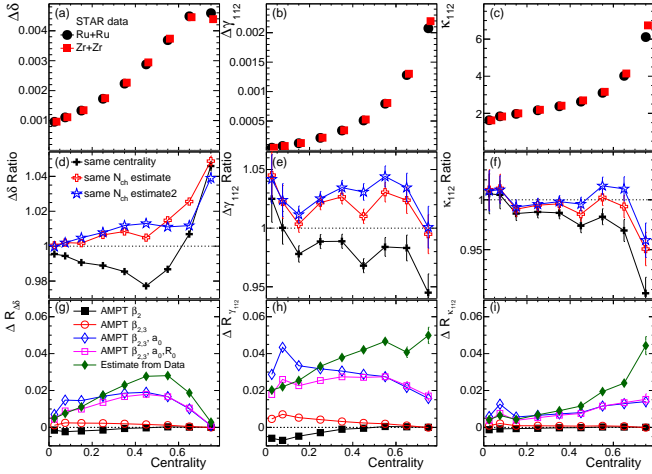


FIG. 5. The results of the CME sensitive observables $\Delta\delta$ (left column), $\Delta\gamma_{112}$ (middle column) and κ_{112} (right column) from isobaric systems. The top row shows the published data. The middle row displays the isobar ratios calculated at matching centrality (filled crosses), and at matching N_{ch} estimated via a linear interpolation from Eq. (2) (open crosses) or via a second-order polynomial interpolation (open stars) labelled as "estimate2". The bottom row shows the ΔR due to switching the event activity variable, based on $p(N_{\text{ch}})$ from the STAR data [1] as well as AMPT including the effects of WS parameters in Eq. (1).

that in Au+Au collisions at 200 GeV [19]. In particular, scaled-variance is set to follow a power-law dependence, $\sigma_{p_T}/\langle p_T \rangle \propto (N_{\text{ch}})^{-n}$, with $n \sim 0.4$ [20]. Motivated by a hydrodynamics argument [21], $\langle p_T \rangle$ undergoes a sharp rise at low N_{ch} [22, 23], followed by a relatively flat behavior in the mid-central region, and then by a second rise in the ultra-central region with an increase of about 10 MeV. The input distributions are shown in the top row of Fig. 6, and are used to estimate the ratio change when switching from matching N_{ch} to matching c .

The bottom panels in Fig. 6 show the change of ratios from matching N_{ch} to matching c via Eq. (3). The insert panel in Fig. 6(c) shows the same $\Delta R_{\langle p_T \rangle}$ but plotted as a function centrality. Since $\langle p_T \rangle$ increases with N_{ch} (or decreases with centrality), the difference $\Delta R_{\langle p_T \rangle}$ is positive according to Eq. 3. Note that if we calculate instead the change of ratio from the same c to the same N_{ch} , as is done in all other figures via Eq. (2), the results would have the opposite signs. $\Delta R_{\langle p_T \rangle}$ reaches a value of ~ 0.0005 at $c = 0.2$, ~ 0.002 at $c = 0.5$, and even larger in more peripheral collisions. This difference is potentially a significant fraction of the signal, $R_{\langle p_T \rangle} - 1$, as a function of centrality, which is predicted to be ~ 0.003 at $c = 0.2$ and ~ 0.005 at $c = 0.5$ in a hydrodynamic model simulation with nuclear structure parameters close to those in Tab. I [12]. The impact of switching the event activity variable is generally smaller in more central collisions. On the other hand, since $\sigma_{p_T}/\langle p_T \rangle$ increases with centrality (or decreases with N_{ch}), the difference in its ratio is negative, with a magnitude of ~ 0.01 at $c = 0.2$, which

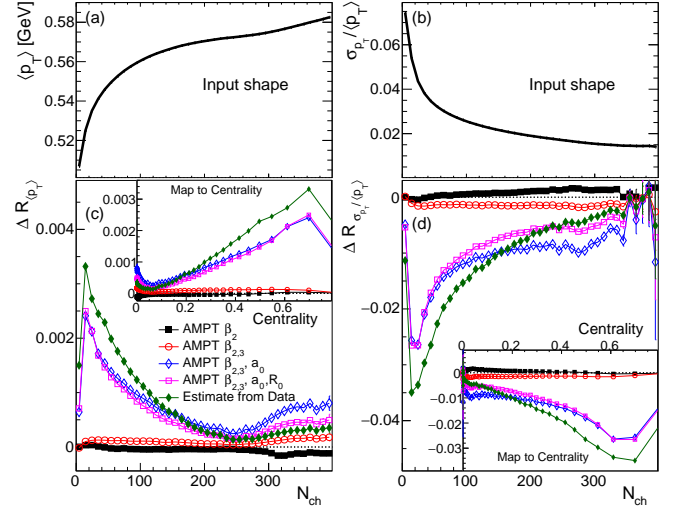


FIG. 6. The input N_{ch} dependence of $\langle p_T \rangle$ (a) and $\sigma_{p_T}/\langle p_T \rangle$ (b), and the corresponding ΔR (change from the ratio at matching centrality) based on the $p(N_{\text{ch}})$ distributions from STAR data and AMPT. The insert panels show the same ΔR after mapping N_{ch} to centrality in the x -axis.

increases to ~ 0.03 at $c = 0.5$. The comparison with the AMPT simulations shows that the difference in the diffuseness parameter between the isobaric systems plays the dominant role.

In the current study, c and N_{ch} are analytically related in each collision system, and the two isobar ratios (at matching c and at matching N_{ch}) are different only because $c(N_{\text{ch}})_{\text{Ru}} \neq c(N_{\text{ch}})_{\text{Zr}}$ in Fig. 1. In general, event activity variables are not analytically related, such as the multiplicity determined at mid-rapidities and that determined at forward rapidities. As a concrete example, one can consider the relation between N_{ch} and N_{EPD} , multiplicity in the STAR event-plane detector at $2 < |\eta| < 5$. In this case, one also has to take into account the fluctuations of N_{EPD} for events with fixed N_{ch} , and vice versa. This effect, also known as volume fluctuations, may lead to additional differences in the isobar ratios [24, 25] (besides that due to switching between c and N_{ch}). Specifically, events from N_{EPD} selection with an average of $\langle N_{\text{ch}} \rangle = N_0$, may not have the same physics signal as events selected directly with a fixed $N_{\text{ch}} = N_0$. The difference could be particularly large for multi-particle cumulant observables [25–27]. A study of this is in progress.

In summary, we have studied how the choice of event activity variable x influences the observable ratio, $R_{\mathcal{O}}(x)$, of $^{96}\text{Ru}+^{96}\text{Ru}$ to $^{96}\text{Zr}+^{96}\text{Zr}$ collisions. Significant deviations of these ratios from unity have been attributed to the different collective nuclear structures of ^{96}Ru and ^{96}Zr nuclei. In addition to directly influencing \mathcal{O} in the two systems, the nuclear structure effects can also influence x and hence cause additional differences in $R_{\mathcal{O}}(x)$. The latter contribution depends on the choice of event activity variable x and the rate of change $\ln'(\mathcal{O}(x))$.

Based on published STAR data, we calculate the difference $\Delta R_{\mathcal{O}}$ between the ratios calculated with two event activity variables: charged-particle multiplicity N_{ch} and centrality c . The ratios of harmonic flow v_n are nearly independent of the analysis methods when calculated at matching N_{ch} (i.e. $R_{v_n}(N_{\text{ch}})$) instead of at matching c (i.e. $R_{v_n}(c)$), suggesting that nonflow effects are controlled by N_{ch} instead of centrality. The isobar ratios for the CME sensitive observable (κ_{112}) are also closer to unity, when the event activity is quantified by N_{ch} instead of c , indicating that the former provides a better estimate of the background baseline for this observable. The AMPT model calculations are used to separate $\Delta R_{\mathcal{O}}$ into different effects of the nuclear structure parameters in the Woods-Saxon form. Surface diffuseness a_0 is

found to have the largest influence, followed by nuclear radius R_0 , and nuclear deformations only influence $\Delta R_{\mathcal{O}}$ in central collisions. We also make a prediction on the expected ΔR for mean transverse momentum ($\langle p_{\text{T}} \rangle$) and its scaled-variance ($\sigma_{p_{\text{T}}}/\langle p_{\text{T}} \rangle$). The difference between the $\langle p_{\text{T}} \rangle$ ratios at matching N_{ch} and at matching centrality is sizeable compared with the total influence of the nuclear structure effects on $R_{\langle p_{\text{T}} \rangle}$. This difference needs to be taken into account explicitly in model calculations.

Acknowledgements: We appreciate comments from Somadutta Bhatta. J. J. and C. Z. are supported by the U.S. Department of Energy under Grant No. DEFG0287ER40331. G. W. is supported by the U.S. Department of Energy under Grant No. DE-FG02-88ER40424.

-
- [1] Mohamed Abdallah *et al.* (STAR), “Search for the chiral magnetic effect with isobar collisions at $\sqrt{s_{NN}}=200$ GeV by the STAR Collaboration at the BNL Relativistic Heavy Ion Collider,” *Phys. Rev. C* **105**, 014901 (2022), [arXiv:2109.00131 \[nucl-ex\]](#).
- [2] Kenji Fukushima, Dmitri E. Kharzeev, and Harmen J. Warringa, “The Chiral Magnetic Effect,” *Phys. Rev. D* **78**, 074033 (2008), [arXiv:0808.3382 \[hep-ph\]](#).
- [3] B. I. Abelev *et al.* (STAR), “Azimuthal Charged-Particle Correlations and Possible Local Strong Parity Violation,” *Phys. Rev. Lett.* **103**, 251601 (2009), [arXiv:0909.1739 \[nucl-ex\]](#).
- [4] Sergei A. Voloshin, “Testing the Chiral Magnetic Effect with Central U+U collisions,” *Phys. Rev. Lett.* **105**, 172301 (2010), [arXiv:1006.1020 \[nucl-th\]](#).
- [5] Jianguo Jia and Chun-Jian Zhang, “Scaling approach to nuclear structure in high-energy heavy-ion collisions,” (2021), [arXiv:2111.15559 \[nucl-th\]](#).
- [6] Chunjian Zhang and Jianguo Jia, “Evidence of Quadrupole and Octupole Deformations in Zr96+Zr96 and Ru96+Ru96 Collisions at Ultrarelativistic Energies,” *Phys. Rev. Lett.* **128**, 022301 (2022), [arXiv:2109.01631 \[nucl-th\]](#).
- [7] Hao-jie Xu, Hanlin Li, Xiaobao Wang, Caiwan Shen, and Fuqiang Wang, “Determine the neutron skin type by relativistic isobaric collisions,” *Phys. Lett. B* **819**, 136453 (2021), [arXiv:2103.05595 \[nucl-th\]](#).
- [8] Jianguo Jia, “Shape of atomic nuclei in heavy ion collisions,” *Phys. Rev. C* **105**, 014905 (2022), [arXiv:2106.08768 \[nucl-th\]](#).
- [9] Fei Li, Yu-Gang Ma, Song Zhang, Guo-Liang Ma, and Qi-Ye Shou, “Impact of nuclear structure on the CME background in $^{96}_{44}\text{Ru} + ^{96}_{44}\text{Ru}$ and $^{96}_{40}\text{Zr} + ^{96}_{40}\text{Zr}$ collisions at $\sqrt{s_{NN}} = 7.7 \sim 200$ GeV from a multiphase transport model,” (2022), [10.1103/PhysRevC.106.014906](#), [arXiv:2201.10994 \[nucl-th\]](#).
- [10] Yicheng Feng, Jie Zhao, Hanlin Li, Hao-jie Xu, and Fuqiang Wang, “Two- and three-particle nonflow contributions to the chiral magnetic effect measurement by spectator and participant planes in relativistic heavy ion collisions,” *Phys. Rev. C* **105**, 024913 (2022), [arXiv:2106.15595 \[nucl-ex\]](#).
- [11] Hanlin Li, Hao-jie Xu, Ying Zhou, Xiaobao Wang, Jie Zhao, Lie-Wen Chen, and Fuqiang Wang, “Probing the neutron skin with ultrarelativistic isobaric collisions,” *Phys. Rev. Lett.* **125**, 222301 (2020), [arXiv:1910.06170 \[nucl-th\]](#).
- [12] Hao-jie Xu, Wenbin Zhao, Hanlin Li, Ying Zhou, Lie-Wen Chen, and Fuqiang Wang, “Probing nuclear structure with mean transverse momentum in relativistic isobar collisions,” (2021), [arXiv:2111.14812 \[nucl-th\]](#).
- [13] Jianguo Jia, “Probing triaxial deformation of atomic nuclei in high-energy heavy ion collisions,” *Phys. Rev. C* **105**, 044905 (2022), [arXiv:2109.00604 \[nucl-th\]](#).
- [14] Giuliano Giacalone, “Observing the deformation of nuclei with relativistic nuclear collisions,” *Phys. Rev. Lett.* **124**, 202301 (2020), [arXiv:1910.04673 \[nucl-th\]](#).
- [15] Benjamin Bally, Michael Bender, Giuliano Giacalone, and Vittorio Somà, “Evidence of the triaxial structure of ^{129}Xe at the Large Hadron Collider,” *Phys. Rev. Lett.* **128**, 082301 (2022), [arXiv:2108.09578 \[nucl-th\]](#).
- [16] Jianguo Jia, Shengli Huang, and Chunjian Zhang, “Probing nuclear quadrupole deformation from correlation of elliptic flow and transverse momentum in heavy ion collisions,” *Phys. Rev. C* **105**, 014906 (2022), [arXiv:2105.05713 \[nucl-th\]](#).
- [17] Zi-Wei Lin, Che Ming Ko, Bao-An Li, Bin Zhang, and Subrata Pal, “A Multi-phase transport model for relativistic heavy ion collisions,” *Phys. Rev. C* **72**, 064901 (2005), [arXiv:nucl-th/0411110 \[nucl-th\]](#).
- [18] Wei Li and Gang Wang, “Chiral Magnetic Effects in Nuclear Collisions,” *Ann. Rev. Nucl. Part. Sci.* **70**, 293–321 (2020), [arXiv:2002.10397 \[nucl-ex\]](#).
- [19] Jaroslav Adam *et al.* (STAR), “Collision-energy dependence of p_t correlations in Au + Au collisions at energies available at the BNL Relativistic Heavy Ion Collider,” *Phys. Rev. C* **99**, 044918 (2019), [arXiv:1901.00837 \[nucl-ex\]](#).
- [20] Betty Bezverkhny Abelev *et al.* (ALICE), “Event-by-event mean p_{T} fluctuations in pp and Pb-Pb collisions at the LHC,” *Eur. Phys. J. C* **74**, 3077 (2014), [arXiv:1407.5530 \[nucl-ex\]](#).
- [21] Fernando G. Gardim, Giuliano Giacalone, and Jean-Yves Ollitrault, “The mean transverse momentum of ultracentral heavy-ion collisions: A new probe of hydrodynamics,” *Phys. Lett. B* **809**, 135749 (2020),

- [arXiv:1909.11609 \[nucl-th\]](#).
- [22] Betty Bezverkhny Abelev *et al.* (ALICE), “Multiplicity dependence of the average transverse momentum in pp, p-Pb, and Pb-Pb collisions at the LHC,” *Phys. Lett. B* **727**, 371–380 (2013), [arXiv:1307.1094 \[nucl-ex\]](#).
- [23] Shreyasi Acharya *et al.* (ALICE), “Transverse momentum spectra and nuclear modification factors of charged particles in Xe-Xe collisions at $\sqrt{s_{NN}} = 5.44$ TeV,” *Phys. Lett. B* **788**, 166–179 (2019), [arXiv:1805.04399 \[nucl-ex\]](#).
- [24] Mingliang Zhou and Jiangyong Jia, “Centrality fluctuations in heavy-ion collisions,” *Phys. Rev. C* **98**, 044903 (2018), [arXiv:1803.01812 \[nucl-th\]](#).
- [25] Morad Aaboud *et al.* (ATLAS), “Fluctuations of anisotropic flow in Pb+Pb collisions at $\sqrt{s_{NN}} = 5.02$ TeV with the ATLAS detector,” *JHEP* **01**, 051 (2020), [arXiv:1904.04808 \[nucl-ex\]](#).
- [26] Tetsuro Sugiura, Toshihiro Nonaka, and Shinichi Esumi, “Volume fluctuation and multiplicity correlation in higher-order cumulants,” *Phys. Rev. C* **100**, 044904 (2019), [arXiv:1903.02314 \[nucl-th\]](#).
- [27] Jiangyong Jia, Chunjian Zhang, and Jun Xu, “Centrality fluctuations and decorrelations in heavy-ion collisions in a Glauber model,” *Phys. Rev. Res.* **2**, 023319 (2020), [arXiv:2001.08602 \[nucl-th\]](#).